Revue-IRS

Revue Internationale de la Recherche Scientifique
(Revue-IRS)
ISSN: 2958-8413
Vol. 3, No. 4, Juillet 2025

HYDRODYNAMICS OF LAKE ITASY: OPTIMIZING A NUMERICAL MODEL FOR STABILITY AND MASS CONSERVATION USING ADAPTIVE COURANT-FRIEDRICHS-LEWY CRITERION

RALIJAONA Herilala Tafitasoloniaina[1], RANDRIANJA Malanto Miangaly[2]

[1] Informatique Department, Water and Environmental Engineering Department, University of Itasy, Soavinandriana, Madagascar
[2] Informatique Department, University of Itasy, Soavinandriana, Madagascar

Abstract: Hydrodynamic modeling of inland water bodies is crucial for effective water resource management, flood forecasting, and environmental monitoring. This study focuses on Lake Itasy, Madagascar, and aims to enhance the numerical stability and mass conservation of a shallow water equation (SWE)-based hydrodynamic model. The methodology combines remote sensing (NDWI on Sentinel-2 imagery), geospatial analysis (SRTM DEM), and numerical simulation, integrating physical processes such as tributary inflows, precipitation, evaporation, wind forcing, and outlet boundary conditions. Satellite data analysis revealed a reduction in lake surface area in 2024 compared to 2023, providing a relevant hydrological context. A key innovation lies in the implementation of an adaptive Courant-Friedrichs-Lewy (CFL) criterion, which dynamically adjusts the time step to maintain stability without compromising computational efficiency. The results demonstrate that a CFL value of 0.01 ensures high accuracy and numerical stability, albeit at the cost of increased computation time. Overall, this work establishes a robust and reliable modeling framework, offering a valuable tool for future hydrological studies and sustainable water management in the Itasy region.

Keywords: Hydrodynamic modeling; Lake Itasy; Adaptive CFL condition; Mass conservation; Numerical stability; Remote sensing; Sentinel-2; Water balance; Geospatial analysis; Numerical viscosity

Digital Object Identifier (DOI): https://doi.org/10.5281/zenodo.**15869419**

1 Introduction

Hydrodynamic modeling of inland water bodies, such as lakes, is an essential tool for water resource management, flood forecasting, water quality assessment, and understanding aquatic ecosystems. The systems of partial differential equations that describe water flow form the foundation of many numerical models used for this purpose [2][6][11]. However, the numerical resolution of these equations presents inherent challenges, particularly concerning numerical stability and mass conservation.

Stability is paramount to ensure that simulations remain physically consistent and do not diverge. Most of the time, the Courant-Friedrichs-Lewy (CFL) criterion is used to determine the maximum admissible time step to ensure

this stability [4][9]. However, applying a fixed time step can either unnecessarily limit the computation speed (if too small) or compromise stability (if too large). Mass conservation, on the other hand, is a fundamental property of any physical system, and its strict adherence by a numerical model is crucial for the reliability of predictions, especially for a lake's water balance over prolonged periods [1]. Artificial volume losses or gains can render simulation results unusable for decision-making.
This project aims to address these challenges by developing and optimizing a numerical model specifically tailored for simulating Lake Itasy. The main goal is to simultaneously improve the model's numerical stability and the accuracy of mass conservation. To achieve this, we will explore the effectiveness of an adaptive CFL criterion, which allows for dynamic adjustment of the time step to maintain stability while optimizing computational efficiency.
Beyond numerical considerations, this work integrates essential physical aspects crucial for realistic modeling. We will include the influence of the lake's tributaries to simulate hydrological inflows, manage the outlet boundary conditions to model outgoing flow, and incorporate meteorological variables into the model.
The application to Lake Itasy provides a concrete case study to validate the improvements made to the model. The results of this study will highlight the importance of rigorous calibration of numerical and physical parameters to obtain robust and accurate hydrodynamic simulations. This will, in turn, provide a solid foundation for future environmental studies and water resource management efforts.

2 GEOSPATIAL STUDY OF LAKE ITASY

It's the third-largest lake in Madagascar, located in the Itasy region, in the central-western part of the country. Lake Itasy is of volcanic origin, surrounded by hills and formations from ancient eruptions, and sits at an altitude of about 1,200 meters. Its surface area is approximately 3,500 hectares, and its depth is relatively shallow, averaging four meters. The lake is fed by several small streams and rivers, which act as its tributaries, while its waters flow out through a natural emissary, the Lily River, which then joins the Sakay River.
Lake Itasy supports various economic activities, including fishing, irrigated agriculture, and tourism, thanks to iconic sites like the Lily Falls and the Amparaky geysers. Ecologically, the lake boasts significant biodiversity, comprising both endemic fish and introduced species.

2.1.1 Delimitation of the study area: Lake Itasy

This methodology relies on the analysis of Sentinel-2 images to assess variations in the surface area of Lake Itasy. It breaks down into several steps:

a) Calculation of the NDWI index [7][8]:

The Normalized Difference Water Index (NDWI) is an indicator used in remote sensing to detect and monitor water bodies from satellite imagery.
It's expressed by the following formula:

$$NDWI = \frac{Green - NIR}{Green + NIR} \quad (1)$$

Where :

- G reen band (often band 3 in Landsat)
- NIR (Near-Infrared): near-infrared (often band 5 or 4)

The NDWI (Normalized Difference Water Index) effectively distinguishes water surfaces from other land cover types. When the NDWI is greater than zero (NDWI > 0), it indicates a high probability of water presence, such as lakes, rivers, or dams. Conversely, an NDWI less than zero (NDWI < 0) suggests the surface is composed of bare soil, vegetation, or urban areas.
For Sentinel-2 images, the NDWI is derived from the green band (B3) and the near-infrared band (B8) to identify pixels corresponding to water surfaces.

b) Lake Surface Mapping :

An NDWI-based water mask is applied to each image to isolate aquatic areas. The lake's surface area is then calculated by multiplying the number of water pixels by their unit area. The results are aggregated to obtain an estimate of the total lake area.

c) Temporal Analysis :

Sentinel-2 images are extracted for each month of the study period (January to December 2024). Only images with less than 30% cloud cover are retained. The calculation of the lake's surface area is applied to each monthly image. The average monthly lake surface area is then calculated from these results.

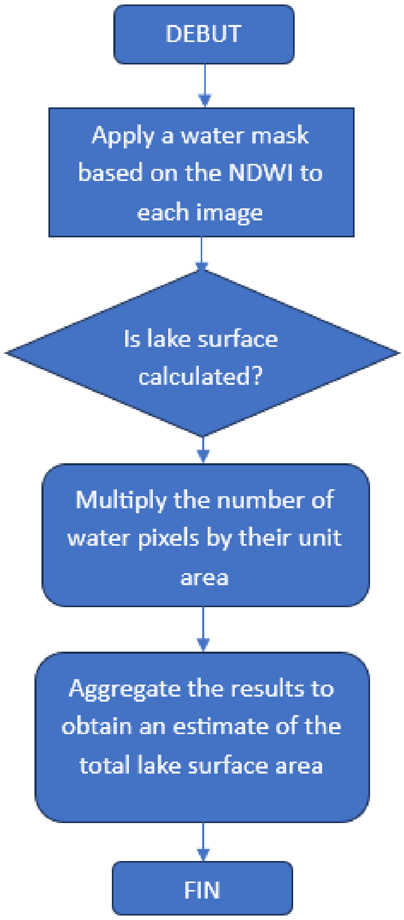

Figure 1. Algorithm for Lake Surface Area Calculation

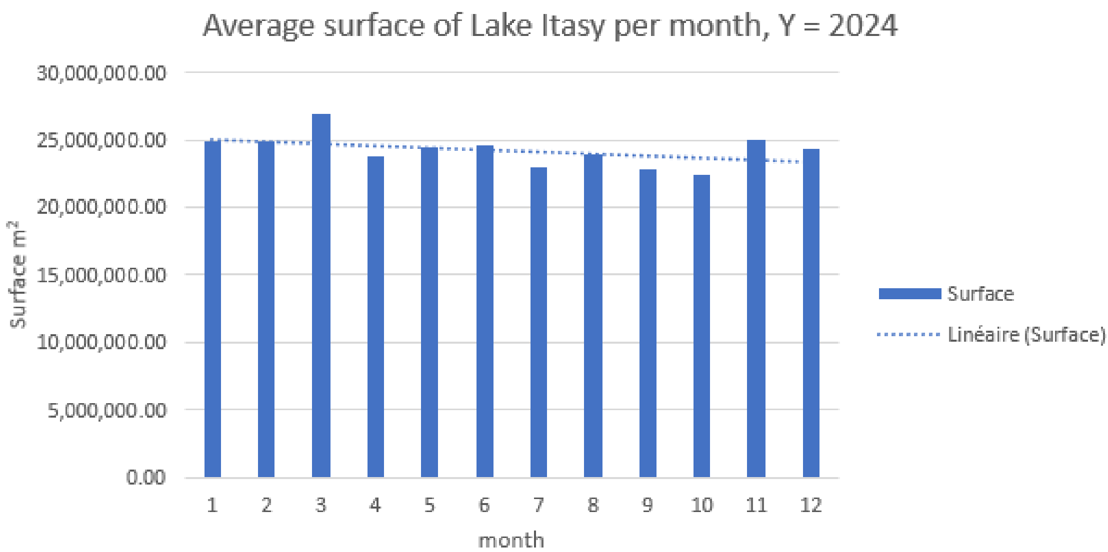

Figure 2. Surface moyenne du lac Itasy par mois

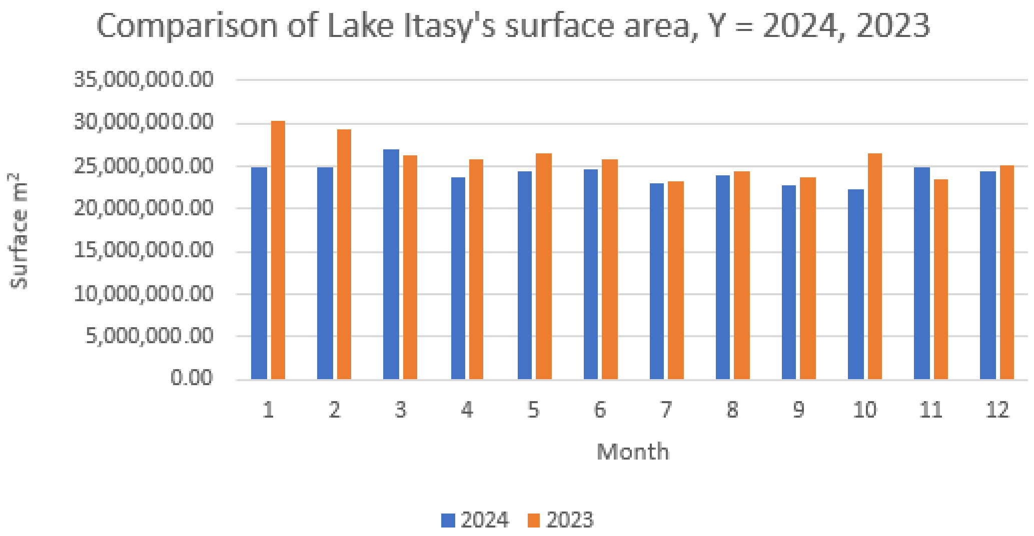

Figure 3. Comparison of Lake Itasy's surface area, Y = 2024, 2023

The analysis of Lake Itasy's surface area reveals a distinct monthly dynamic, with significant variations throughout 2024. We observe a notable increase in surface area at the beginning of the year, peaking in February and March, which suggests a period of heavy rainfall or significant water inflows. Conversely, July and October are characterized by a decrease in surface area, potentially indicating drought conditions or increased evaporation.
Overall, a trend emerges: a gradual increase in surface area at the beginning of the year, followed by a continuous decrease until October, then a slight rise towards the end of the year. The trend curve is slightly downward. This gentle slope indicates a minor decrease in the surface area throughout 2024.
Figure 3 indicates that Lake Itasy had a significantly larger surface area for most of 2023 compared to 2024. This suggests that 2023 was either a rainier year or experienced more consistent water input, leading to a higher water level in the lake.

2.1.2 Delimitation of Watersheds

The standard and correct method for calculating flow accumulation and deriving watersheds is based on a Digital Elevation Model (DEM) [5]. To analyze the topography around Lake Itasy, we initially integrated a DEM from the SRTM (Shuttle Radar Topography Mission). This DEM provides a spatial resolution of approximately 30 meters, offering detailed altimetric information essential for calculating slopes and terrain aspect in the study region. Our method involves the following steps:

a) Fill sinks

DEMs often contain "sinks" or local depressions that interrupt flow. We filled these to ensure continuous flow across the landscape.

b) Flow direction calculation

Once the depressions are filled, the next step involves determining the direction in which water flows from each cell in the DEM to its neighbors. The most common algorithm for this is the D8 (Eight-Direction), or sometimes D-Infinity. This function returns an image where each pixel contains the code for the flow direction towards one of its eight neighbors.

c) Flow Accumulation calculation

Using the flow direction image, we can calculate flow accumulation. Flow accumulation for a given cell represents the number of upstream cells that flow into it. The flow direction image (and potentially a weight mask) is used to calculate and then produce an image where each pixel contains the value of the flow accumulation. Areas with high accumulation generally correspond to watercourses.

d) Watershed Delineation :

Once flow accumulation is calculated, we can delineate watersheds by selecting one or more pour points (points where water exits the area of interest). Using the flow accumulation image and these pour points, we can then trace the upstream areas that contribute flow to those specific points.

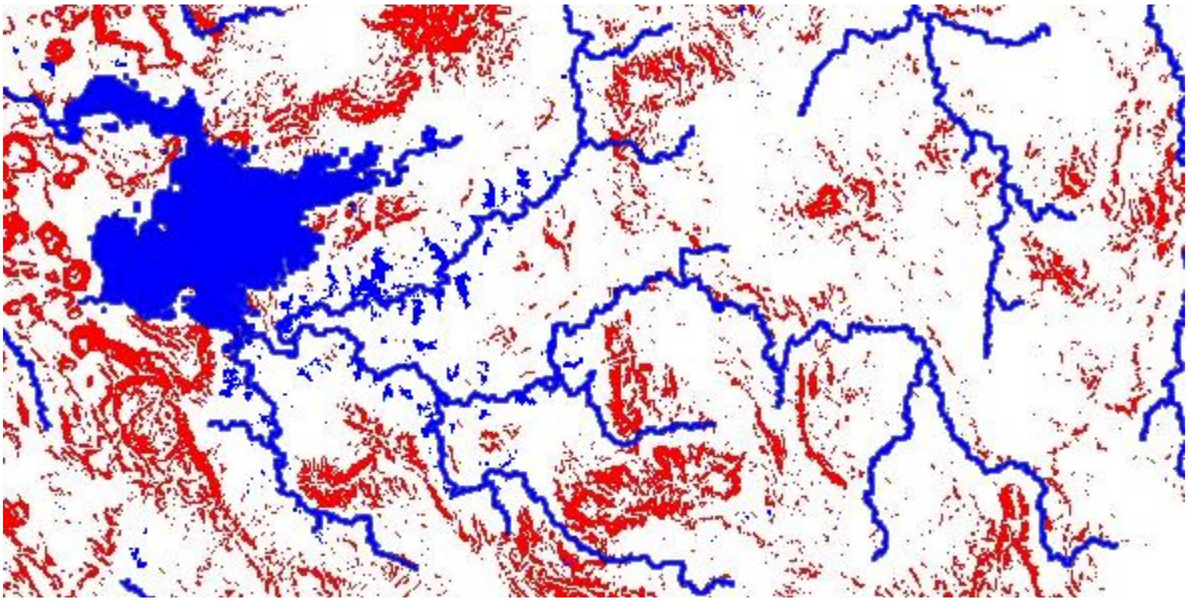

Figure 4. Digital elevation model of the terrain + Water Mask

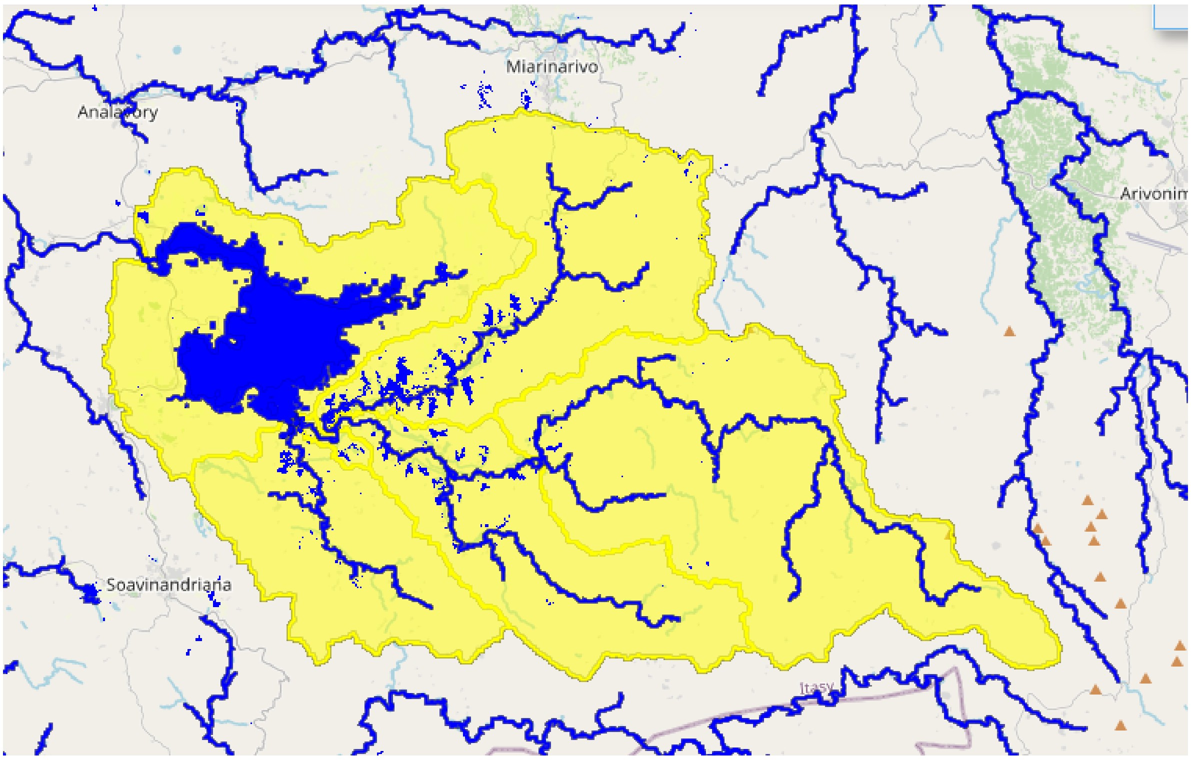

Figure 5. Delineation of the Lake Itasy Watershed

3 METHODOLOGY

3.1 Hydrodynamic model

A hydrodynamic model allows us to simulate currents and water level variations in Lake Itasy. It accounts for various water inputs, such as precipitation and tributary rivers, as well as losses due to evaporation and outflows. By integrating these parameters, it offers a better understanding of water circulation and lake level fluctuations based on meteorological conditions, thus facilitating the analysis of hydrological dynamics and their impact on the ecosystem.

In our study, we used the shallow water equations because the average water depth is negligible compared to the horizontal scale of flow variations [2][11]:

$$\frac{h}{H} << 1 \tag{2}$$

Where :

- h : average water depth

- L: characteristic horizontal length (distance over which the flow varies)

3.2 Bathymetry of Lake Itasy

After measuring the depth of Lake Itasy at several strategic points, we developed an approach to generate a complete bathymetry. This involved establishing key parameters such as the maximum observed depth and the spatial limits defining the shoreline as well as the transition zone towards deeper areas. For each identified location within the lake's perimeter, we calculated its distance from the coastline.

In the littoral zone, delimited by a threshold distance, we determined the depth by gradually increasing it from an initial value to a slightly higher one, while adding a slight random variation to mimic natural bottom irregularities. Beyond this coastal zone, we evolved the depth more progressively and according to a non-linear (cosine) function, thus ensuring a smooth transition to the lake's maximum depth as the distance from the shore increased up to a certain threshold. A slight random variability was also integrated into this deeper zone.

Finally, for each point located inside the lake, we recorded the calculated depth in a matrix, thus constructing a numerical representation of the simulated bathymetry of Lake Itasy, based on its coastal morphology and our initial measurements.

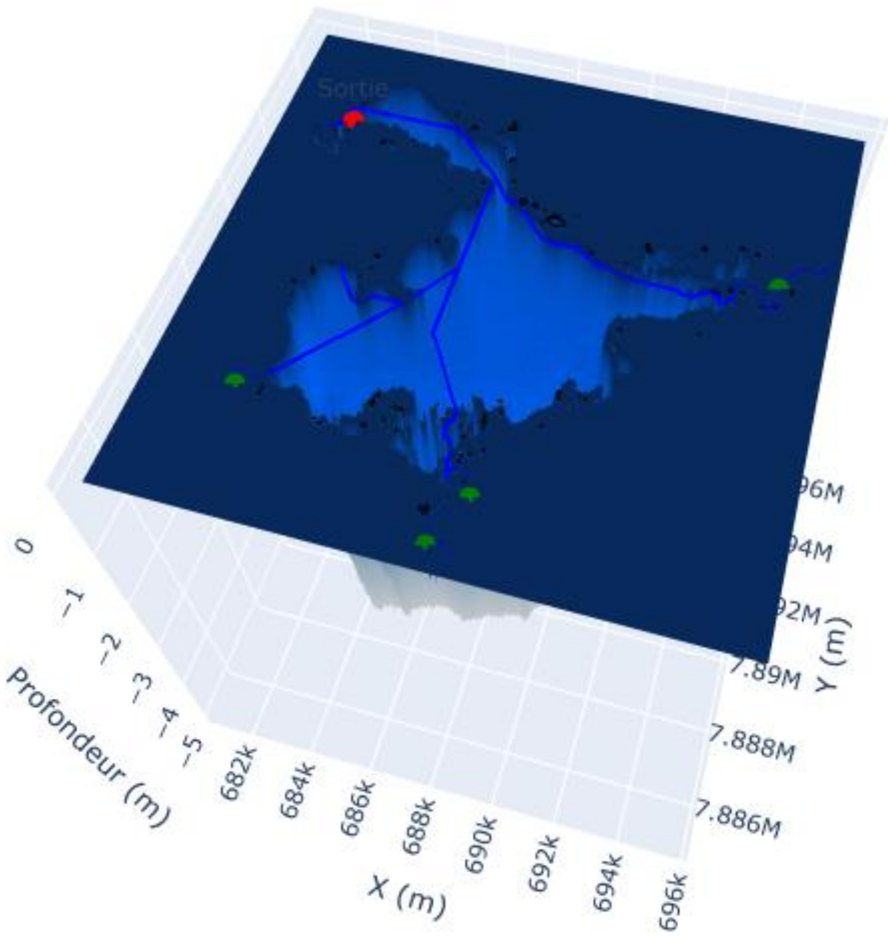

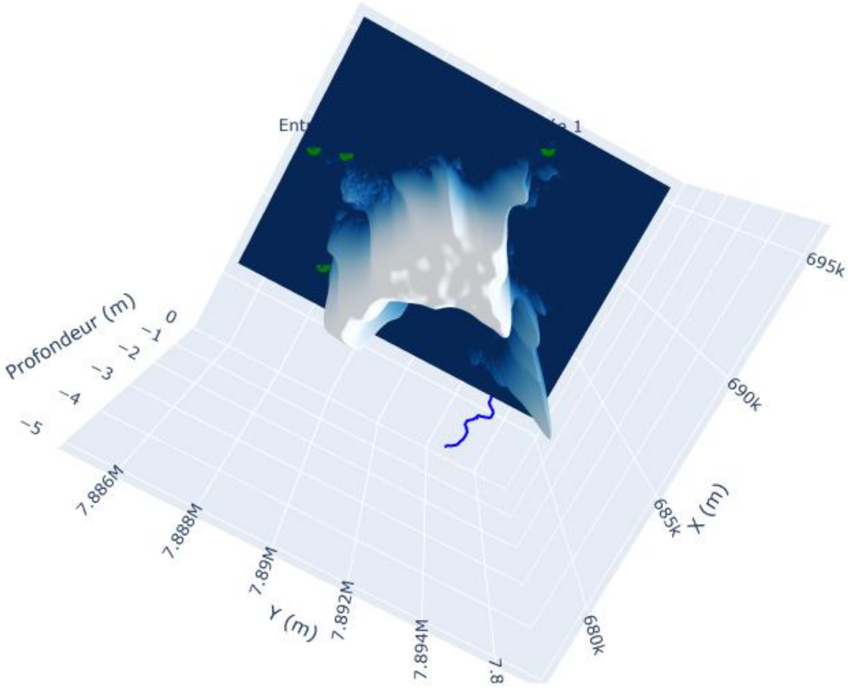
Profondeur (m)
0
−1
−2
−3
−4
−5
7.886M
7.888M
7.89M
7.892M
7.894M
Y (m)
695k
690k
685k
680k
X (m)

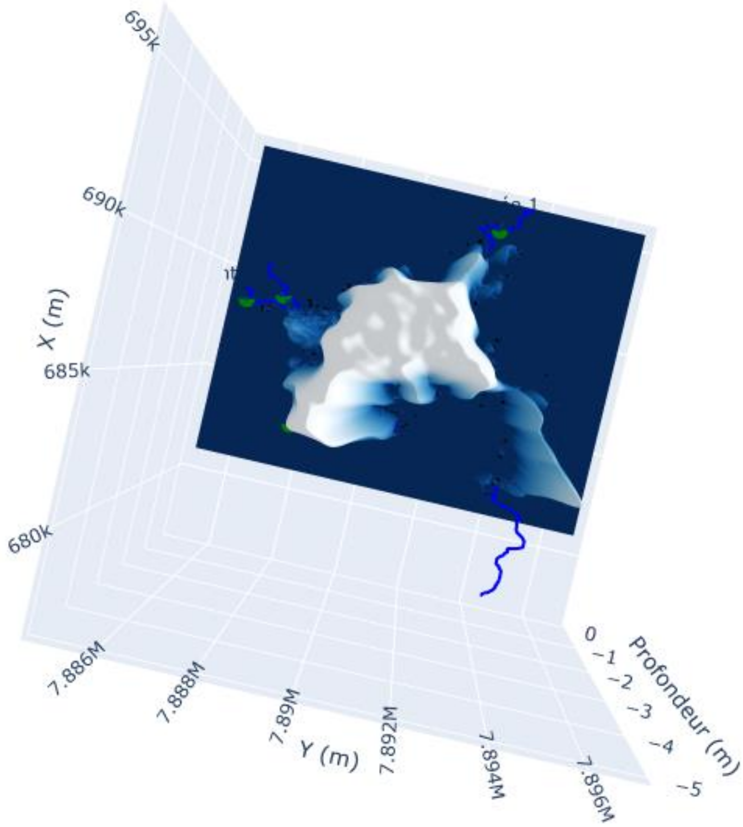
695k
690k
685k
680k
X (m)
7.886M
7.888M
7.89M
7.892M
7.894M
7.896M
Y (m)
0
−1
−2
−3
−4
−5
Profondeur (m)

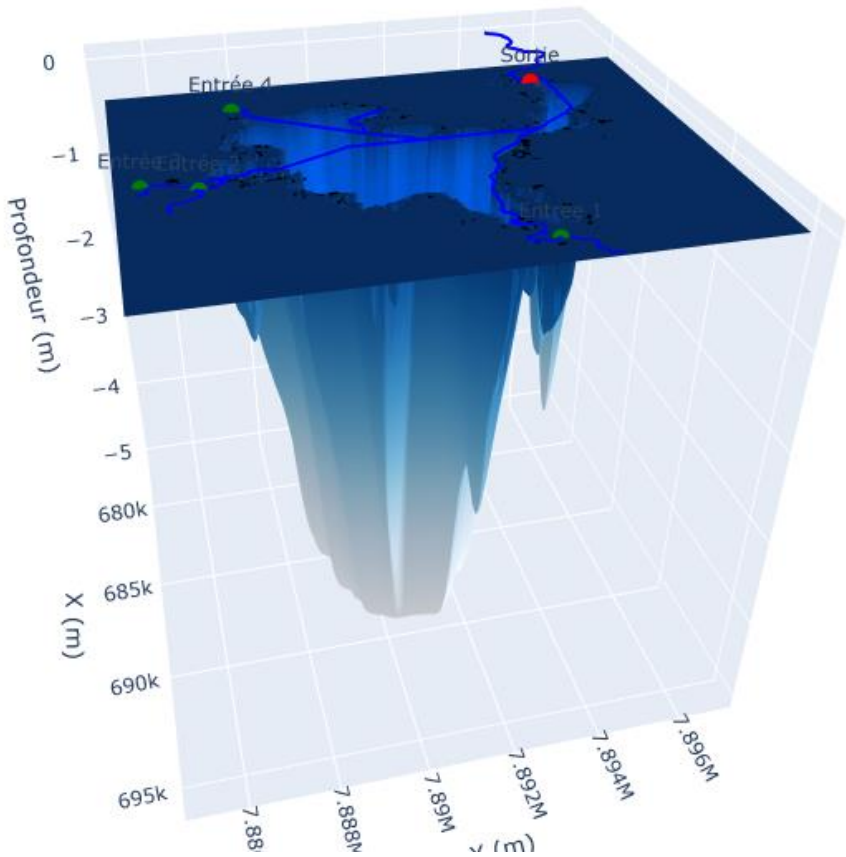

Figure 6. 3D Bathymetry Model of Lake Itasy

3.3 Construction of the conceptual and mathematical model

The model implemented in our study is base d on the Shallow Water Equations (SWE).

- ❖ Approximation by finite differences for numerical resolution

The shallow water equations are formulated in a continuous space and time. To solve them numerically, we've discretized this continuous domain into a finite number of points (the grid) and time intervals [4][6].
For a discretized function $f_{i,j}$ on a 2D grid with step sizes of Δx in the x direction and Δy in the y direction, the components of the gradient $\nabla f = \left(\frac{\partial f}{\partial x}, \frac{\partial f}{\partial y}\right)$ can be approximated as follows:
Centered differences (for interior points):

- ❖ Partial derivative with respect to x:

$$\left.\frac{\partial f}{\partial x}\right|_{i,j} \approx \frac{f_{i,j+1} - f_{i,j-1}}{2\Delta x} \tag{3}$$

- ❖ Partial derivative with respect to y:

$$\left.\frac{\partial f}{\partial y}\right|_{i,j} \approx \frac{f_{i,j+1} - f_{i,j-1}}{2\Delta y} \tag{4}$$

Forward differences (at the left or lower boundary):

- ❖ Partial derivative with respect to x:

$$\left.\frac{\partial f}{\partial x}\right|_{i,0} \approx \frac{f_{i,1} - f_{i,0}}{\Delta x} \tag{5}$$

- ❖ Partial derivative with respect to y:

$$\left.\frac{\partial f}{\partial y}\right|_{o,j} \approx \frac{f_{1,j} - f_{0,j}}{\Delta y} \tag{6}$$

Backward differences (at the right or upper boundary):

❖ Partial derivative with respect to x:

$$\left.\frac{\partial f}{\partial x}\right|_{i,N_x-1} \approx \frac{f_{i,N_x-1} - f_{i,N_x-2}}{\Delta x} \tag{7}$$

❖ Partial derivative with respect to y:

$$\left.\frac{\partial f}{\partial y}\right|_{N_y-1,j} \approx \frac{f_{N_y-1,j} - f_{N_y-2,j}}{\Delta y} \tag{8}$$

Where N_x is the number of points in the x and N_y s the number of points in the y direction.

❖ Tributary Modeling :

For each tributary, the added volume is represented by the following formula :

$$V_{in} = Q_{in}.\Delta t \tag{9}$$

And this volume is distributed over N cells around the entry point by the equation:

$$\Delta h = \frac{V_{in}}{N\,.\Delta x.\ \Delta y} \tag{10}$$

❖ Effluent Modeling

The empirical outflow will be represented by the following formula :

$$Q_{out} = \begin{cases} C.L.\ (h_{exutoire} - h_s)^{\frac{3}{2}}\ , si\ h_{moy} > h_s \\ 0\ ,\ \ sinon \end{cases} \tag{11}$$

Where C : discharge coefficient

L : ffluent width and h_s threshold (minimum level for water to flow)

$h_{\ exutoire}$: lake level at the outfall.

The volume to be removed is defined by:

$$\Delta V = Q_{out}.\Delta t \tag{11}$$

which is distributed proportionally to the height in the outfall area

❖ Diffusion of velocities via the Laplacian: finite difference discretization

$$\nabla^2 u \approx \frac{u_{i,j+1} + u_{i,j-1} + u_{i+1,j} + u_{i-1,j} - 4u_{i,j}}{\Delta x^2 + \epsilon} \tag{12}$$

$$\nabla^2 v \approx \frac{v_{i,j+1} + v_{i,j-1} + v_{i+1,j} + v_{i-1,j} - 4v_{i,j}}{\Delta y^2 + \epsilon} \tag{13}$$

❖ Water level update using the discretized continuity equation

$$h_{i,j}^{(n+1)} = h_{i,j}^{(n)} - \Delta t.\left(\frac{\partial(hu)}{\partial x} + \frac{\partial(hv)}{\partial y}\right)_{i,j}^{(n)} \tag{14}$$

Where the index indicates the value at the current time step.

For the cells where $M_{i,j}$ = 1

$$\left.\frac{\partial(hu)}{\partial x}\right|_{i,j} \approx \frac{(hu)_{i,j+1} - (hu)_{i,j-1}}{2\Delta x}$$
$$\left.\frac{\partial(hv)}{\partial y}\right|_{i,j} \approx \frac{(hv)_{i+1,j} - (hv)_{i-1,j}}{2\Delta y} \tag{15}$$

We should note that $M_{i,j} = h_{i,j} > 0$: refers to the specific value of the lake mask for the cell located at row i and column j. We set $M_{i,j} = 1$ to 1 if water is present, and 0 otherwise.

❖ Including the effect of wind on the lake surface **[3]** :

The wind surface stress τ_w can be modeled as

$$\tau_w = \rho_a C_d |W| W \tag{16}$$

Where ρ_a is the density of air, C_d is the drag coefficient (generally between 10^{-3} et 3×10^{-3} , W is the wind velocity vector above the water surface, and $|W|$ s its scalar magnitude.

This stress can be decomposed into x and y components using the wind direction:

$$\tau_{wx} = \tau_w \cos(\theta_{w)}$$
$$\tau_{wy} = \tau_w \sin(\theta_{w)} \tag{17}$$

Where θ_w is the angular direction of the wind relative to the x-axis (typically measured counter-clockwise from the positive x-axis).
The bed friction shear stress is:

$$\tau_b = \rho_e g \frac{n^2 |U| U}{H^{\frac{4}{3}}} \tag{18}$$

ρ_e : is the density of water (kg/m^3)
n : is the Manning roughness coefficient ($s.m^{-\frac{1}{3}}$)
$|U|$: is the magnitude of the horizontal flow velocity.
U is the velocity vector (u,v).
H is the water depth (m)
Then, to obtain the x and y components:

$$\tau_{bx} = \rho g \frac{n^2 u \sqrt{u^2 + v^2}}{H^{\frac{4}{3}}}$$
$$\tau_{by} = \rho g \frac{n^2 v \sqrt{u^2 + v^2}}{H^{\frac{4}{3}}} \tag{19}$$

❖ Discretized X-Momentum equation, for X-Velocity update

$$u_{i,j}^{(n+1)} = u_{i,j}^{(n)} - \Delta t \,.\left(u_{i,j}^{(n)} \frac{\partial u^n}{\partial x} + v_{i,j}^{(n)} \frac{\partial u^{(n)}}{\partial y} + g \frac{\partial h^{(n)}}{\partial x} + \frac{\tau_{bx}}{\rho} - \frac{\tau_{wx}}{\rho} - \nu \nabla^2 u^{(n)} \right)_{i,j} \tag{20}$$

For cells where $M_{i,j} = 1$

- Advective terms: $u \frac{\partial u}{\partial x} + v \frac{\partial u}{\partial y}$
- Pressure term: $g \frac{\partial h}{\partial x}$
- Viscosity term: $\nu \nabla^2 u$

❖ Discretized Y-Momentum equation, for Y-Velocity update:

$$v_{i,j}^{(n+1)} = v_{i,j}^{(n)} - \Delta t \,.\left(u_{i,j}^{(n)} \frac{\partial v^n}{\partial x} + v_{i,j}^{(n)} \frac{\partial v^{(n)}}{\partial y} + g \frac{\partial h^{(n)}}{\partial y} + \frac{\tau_{by}}{\rho} - \frac{\tau_{wy}}{\rho} - \nu \nabla^2 v^{(n)} \right)_{i,j} \tag{21}$$

For cells where $M_{i,j} = 1$

- Advective terms: $u \frac{\partial v}{\partial x} + v \frac{\partial v}{\partial y}$
- Pressure term: $g \frac{\partial h}{\partial y}$
- Viscosity term : $\nu \nabla^2 v$

In the preceding formulas, we have :

- n is the time step index.
- i, j are the grid cell indices.
- Δt is the time step
- v is the viscosity coefficient

❖ Integration of hydrometeorological processes :

By integrating additional hydrological processes such as evapotranspiration and precipitation into our model, the continuity equation becomes:

$$h_{i,j}^{(n+1)} = h_{i,j}^{(n)} - \Delta t.\left(\frac{\partial(hu)}{\partial x} + \frac{\partial(hv)}{\partial y}\right)_{i,j}^{(n)} + P.\Delta t - E.\Delta t \tag{22}$$

P and E are rates, expressed in units of length per unit of time (mm/day).

3.4 Numerical implementation of the model

3.4.1 Initial conditions and spatial discretization

Once the geographical boundaries of interest are defined in our simulation, the next step is the spatial discretization of the space to allow for numerical calculations. This is achieved by creating a regular grid (or mesh) that overlays the study area. The spatial resolution of our simulation has been set to 200. This means that the mesh will be composed of 200 points along the X-axis and 200 points along the Y-axis, thus forming a total of 200 × 200 = 40,000 cells or grid nodes.
At the beginning of the simulation, the initial conditions and grid properties are defined as:
$g = 9{,}81 m/s^2$: acceleration due to gravity
$h_{(i,j)}^{0} = depth\_matrix_{i,j}$: Initial water depth at cell (i,j). This variable represents the depth or height of the water column above the bottom at the very beginning of the simulation for each grid cell (i,j).
$u_{(i,j)}^{0} = 0$: initializes the x-component of the water's velocity to zero for each cell at the start of the simulation. This means the water is initially stationary in the x-direction.
$v_{(i,j)}^{0} = 0$: defines that the water is initially stationary in the Y-direction.
It can also be noted that:

$$u_{i,j}^{(n+1)} = 0, v_{i,j}^{(n+1)} = 0, h_{i,j}^{(n+1)} = 0 \; si \; M_{i,j} = 0 \tag{22}$$

$\Delta x = X_{0,1} - X_{0,0}$: This value represents the width of a single computational grid cell in the X direction. It's obtained by calculating the difference between the X-coordinates of two neighboring grid points. This assumes that the grid is regular, with cells of constant size in the X direction.
$\Delta y = Y_{0,1} - Y_{0,0}$: we assume the grid is regular, with cells of constant size in Y.
$\varepsilon = 10^{-9}$: for numerical stability by avoiding division-by-zero errors, which could occur if Δx or Δy become zero or extremely small.
$ox_{idx} = \arg min_j \left|X_{0,j} - outlet\_coord_x\right|$: This formula determines the column index of the grid (along the X-axis) that is closest to the specified X-coordinate for the outfall (the lake's water outlet).
$oy_{idy} = \arg min_j \left|Y_{0,j} - outlet\_coord_y\right|$: similarly, this relationship finds the row index of the grid (along the Y-axis) closest to the outfall's Y-coordinate.

3.4.2 Dynamic time step adaptation according to the CFL criterion

In our simulation, a crucial method for ensuring computational stability and efficiency is the dynamic adaptation of the time step based on the Courant-Friedrichs-Lewy (CFL) number. This approach is fundamental in the numerical solution of partial differential equations, as it allows the model to adjust to the changing physical conditions of the system and prevent numerical instabilities.
The logic for dynamically adjusting the time step is implemented at the beginning of each step in the simulation loop.

❖ Calculation of characteristic velocities :

✓ Speed of gravity waves (c) :

For each lake cell, the propagation speed of small disturbances (waves) is calculated by:

$$c = \sqrt{g \, . h} \tag{23}$$

where g is the acceleration due to gravity and h is the water depth in the cell. This is the speed at which water level change information propagates.

✓ Total current velocity

The magnitude of the current velocity is calculated as:

$$abs_{u_{total}} = \sqrt{u^2 + v^2} \tag{24}$$

where u and v are the velocity components in the x and y directions, respectively.

❖ Determining the CFL Time step per cell

For each active lake cell, the maximum allowed time step $\Delta t_{CFL_{i,j}}$ for this cell is calculated using the sum of the current velocity and the gravity wave speed. This represents the fastest propagation speed of information within that cell:

$$\Delta t_{CFL_{i,j}} = cfl_{safety_{factor}} \cdot \frac{\Delta x}{abs_{u_{total}} + c + \epsilon_{vitesse}} \tag{25}$$

, where $cfl_{safety_{factor}}$ is a safety factor: set to 0.1, 0.4, and then 0.8 in our case. It's always less than 1 and is used to keep the CFL number well below the critical limit, thereby increasing stability but potentially increasing computation time.

Δx : represents the mesh cell size

$\epsilon_{vitesse}$: is a small numerical value (1e-6) added to prevent division by zero if velocities and c are zero.

❖ Global time step selection

Since the simulation must be stable for all cells in the mesh, the time step for the next step is chosen as the minimum value of: $\Delta t_{CFL_{i,j}}$ calculated over the entire lake.

$$\Delta t_{new} = \min_{(i,j)\in M_{i,j}=1} (\Delta t_{CFL_{i,j}}) \tag{26}$$

This ensures that even the cell with the fastest information propagation remains stable. The algorithm also makes sure that the time step does not exceed the remaining time before the end of the simulation, ensuring it finishes precisely at the target duration.

4 METRICS

To evaluate the model's stability, several metrics were observed. In this context, stability means that the simulation doesn't diverge numerically and that it produces physically plausible results. For example, water height or velocity values don't become infinite or oscillate in a non-physical way.

4.1 Conservation of mass (Water volume):

The total water volume over time is calculated by summing the water depth (multiplied by the area of each cell) over all cells where the water mask is positive.

Initially, we configure the system as a closed system, meaning there are no sources or losses (other than the outfall and controlled tributaries). The total water volume should be conserved (apart from intentional additions and removals later in the simulation). A drastic and unexplained increase or decrease in total volume indicates instability. The relative variation of the total water volume over time is given by the following relationship:

$$Variation\ relationship = \frac{|Volume(t) - Volume\ (t-1)|}{Volume(t-1)} \tag{26}$$

4.2 Physical values of variables

During hydrodynamic simulations, certain numerical indicators help us assess the model's stability and realism.

- **Water level (h):** The water depth must remain positive or zero (if a cell dries out). Negative values are a sign of numerical instability. Wild and non-physical oscillations in water depth are also problematic.

- **Velocity (u, v):** velocities must remain within physically reasonable limits for the system. Excessively high and sudden velocity values are often a sign of instability.

4.3 Courant-Friedrich-Lewy criterion (CFL) [4]

The CFL (Courant-Friedrichs-Lewy) condition is a numerical stability condition for methods used to solve partial differential equations, especially advection or transport equations.

It imposes a relationship between the time step (Δt) and the spatial step (Δx, Δy), ensuring that physical information (fluid) does not traverse more than one mesh cell per time step.

$$CFL = \frac{u\,.\Delta t}{\Delta x} < 1 \tag{27}$$

u : flow velocity

Δt: time step

Δx : Cell size (spatial mesh)

In 2D or 3D, we generalize as follows:

$$CFL = \left|\frac{u\,.\Delta t}{\Delta x}\right| + \left|\frac{u\,.\Delta t}{\Delta y}\right| + \cdots \leq C_{max} \tag{28}$$

C_{max} : limit value that the Courant (CFL) number must not exceed for the numerical scheme to remain stable.

C_{max} should ideally remain less than 1.

Δx et Δy : are the sizes of our grid.

5 RESULTS AND DISCUSSIONS

The simulation is set up using several physical and control constants. These include a Manning's roughness coefficient (n=0.02), the gravitational constant (g=9.81 m/s2), a minimum water depth ($h_{min}=10^{-6}$ m) to prevent division by zero. An outfall threshold of 0.64 m regulates water outflow. The simulation runs on a 200×200 grid with an initial time step of 4 s, for a total simulation duration of one day. The lake's four tributaries are defined by their geographical coordinates (longitude, latitude):

- (46.84690312179199,-19.05071684269793)
- (46.79676394057938,-19.105227065959568),
- (46.791612654838374, -19.114959145984137),
- (46.74044321647758, -19.096143274629064).

These coordinates are then transformed into the EPSG:32738 projected coordinate system for use with the simulation grid. The outfall (outlet) is located at geographical coordinates (46.73711, -19.03389), also transformed into EPSG:32738 projected coordinates. Water outflow through the outfall only occurs if the water depth in the outfall cell exceeds a threshold of 0.64 m. The parameters used for calculating the outflow rate are an outfall width of 4.0 m and a discharge coefficient of 0.6.

5.1 Comparative analysis of time step evolution based on the CFL Factor

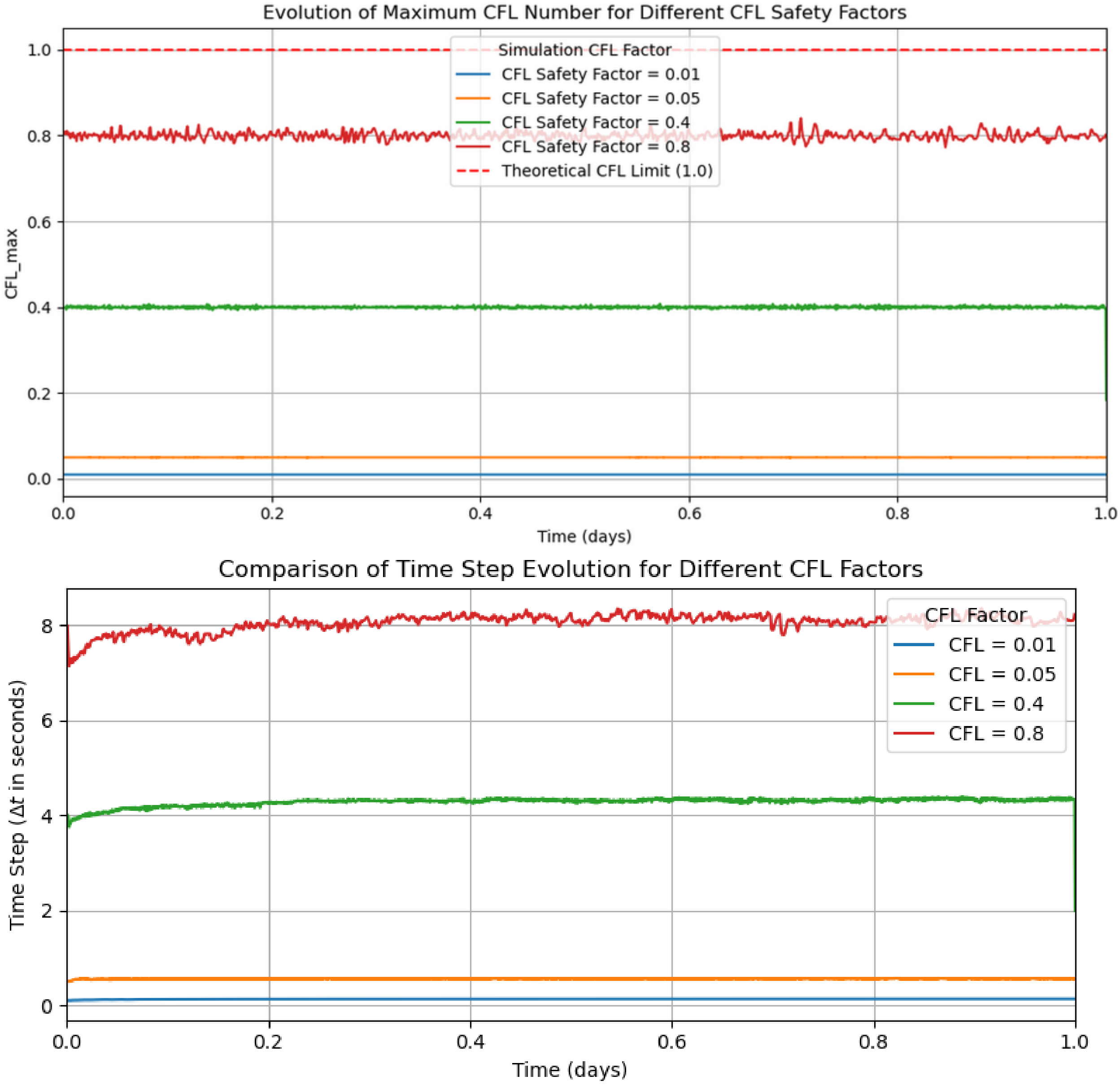

Figure 7. Evolution of CFL and time step during the simulation

The first graph shows that the calculated CFL number is consistently maintained around the defined value of $cfl_{safety_{factor}}$. This confirms that our adaptive CFL algorithm is working correctly. It dynamically adjusts the time step to ensure the CFL number doesn't exceed the specified safety value, which is well below the instability threshold of 1.0. This guarantees the numerical stability of the simulation, even with a higher safety factor that potentially allows for larger time steps than if a factor of 0.01 had been used. It's also worth noting that the other model parameters don't alter the CFL factor's ability to stabilize at its nominal value.

However, for the simulation with a factor $cfl_{safety_{factor}}$ of **0.8**, we observe greater instability in the time step's evolution. This is unlike other cases where the time step stabilizes quickly. Even if the simulation doesn't completely diverge with this value, the oscillations mean that the calculation is less efficient and could present risks of divergence and instability during a prolonged simulation over a longer duration.

5.2 Comparative analysis of time step distribution based on the CFL Factor

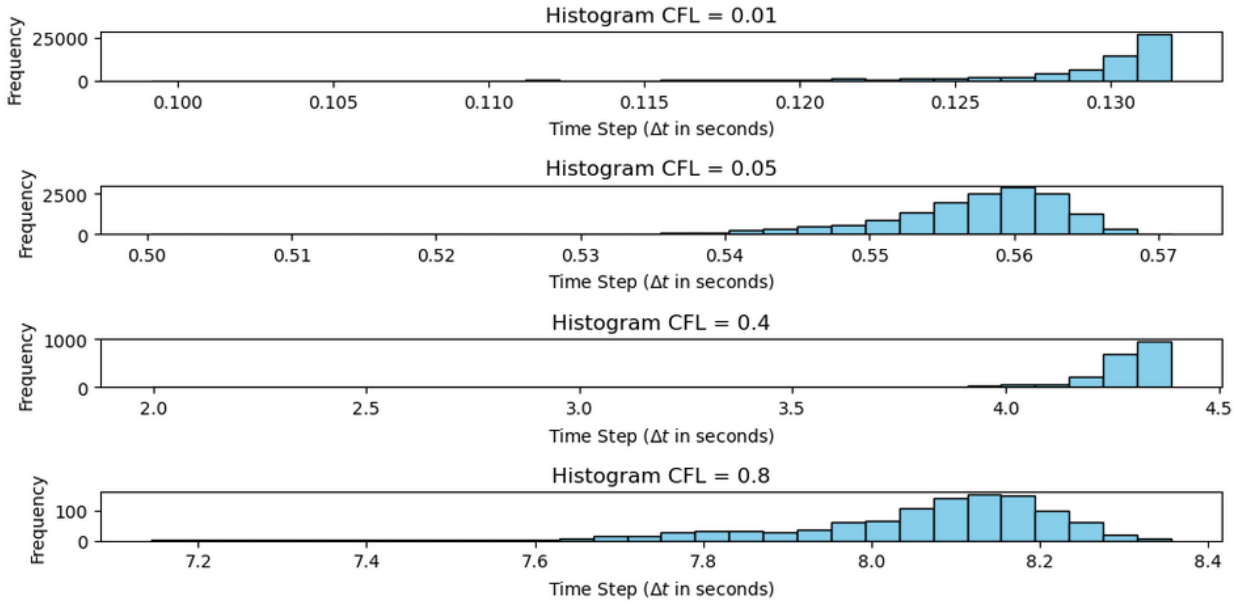

Figure 8. Distribution of time steps based on the defined CFL

For a CFL factor of **0.01**, the Δt (time step) values are **highly concentrated around small values**, primarily between 0.125 and 0.1337 seconds. The most frequent occurrence, or peak, is around 0.132 seconds, with a maximum frequency reaching approximately 25,000 occurrences for the most frequent bin. This represents the **most conservative case**, where the time step is consistently kept very small. This confirms the **high numerical stability** previously mentioned, but it also indicates a **very slow simulation** due to the large number of small steps taken. The **narrow distribution** further suggests that the time step's evolution over time is **very stable and not prone to significant fluctuations.**

For a CFL factor of **0.05**, the Δt (time step) values are **larger** than for CFL=0.01, primarily ranging between 0.54 and 0.57 seconds, with a peak around 0.56 seconds. The maximum frequency reaches approximately 2,500 occurrences for the most frequent bin. It's important to note that the frequency scale has changed significantly compared to the CFL=0.01 graph (decreasing from 25,000 to 2,500), which indicates a **much smaller total number of steps** for the same simulation duration. The distribution remains relatively narrow and well-defined, suggesting that the time step remained quite stable most of the time, although there's a slight "tail" towards smaller values (0.50-0.54), representing initial and sporadic adjustments.

For a CFL factor of **0.4**, the Δt (time step) is even larger, centered around 4.0 to 4.3 seconds, with a clear peak just above 4.0 seconds. The maximum frequency drops to approximately 1,000 occurrences for this peak. The frequency scale continues to decrease, confirming that fewer steps are needed for the simulation. Considering this parameter alone, this represents an excellent compromise. The time step is significantly higher, which considerably speeds up the simulation. The distribution is still quite concentrated, indicating that the time step remains relatively stable, although there are occurrences of slightly smaller time steps (around 4.0-4.1) and larger ones (4.3-4.4). This variation is typical of effective adaptive adjustment.

For a CFL factor of **0.8**, the Δt (time step) values are the largest, but the distribution is notably broader and less sharply peaked. Values range from approximately 7.2 seconds to 8.4 seconds, with several high-frequency bars rather than a single, dominant peak. The maximum frequency is the lowest (around 150 occurrences), confirming that the total number of steps is minimal, resulting in a faster simulation.

This histogram better supports the observation of the more significant oscillations seen in the previous graph (Figure 7). The broadening of the distribution indicates that the time step cannot stabilize on a single, dominant value. Instead, it fluctuates frequently within a wider range. This reinforces the idea that the model is operating very close to its stability limits for this CFL value, even if the simulation hasn't diverged (which would be characterized by Δt values dropping to zero or calculation errors).

5.3 Comparison of water level evolution at the outfall

The following graph illustrates the evolution of water depth at the outfall of our simulated system over a 24-hour period, considering different CFL safety factors.

The simulation starts with a very large initial lake volume of 107,874,726.210321 m³. There's also a constant inflow of 0.8 m³/s (0.2 m³/s from each of the four tributaries), which adds up to 69,120 m³ over 24 hours. This inflow represents about 0.064% of the lake's initial volume.

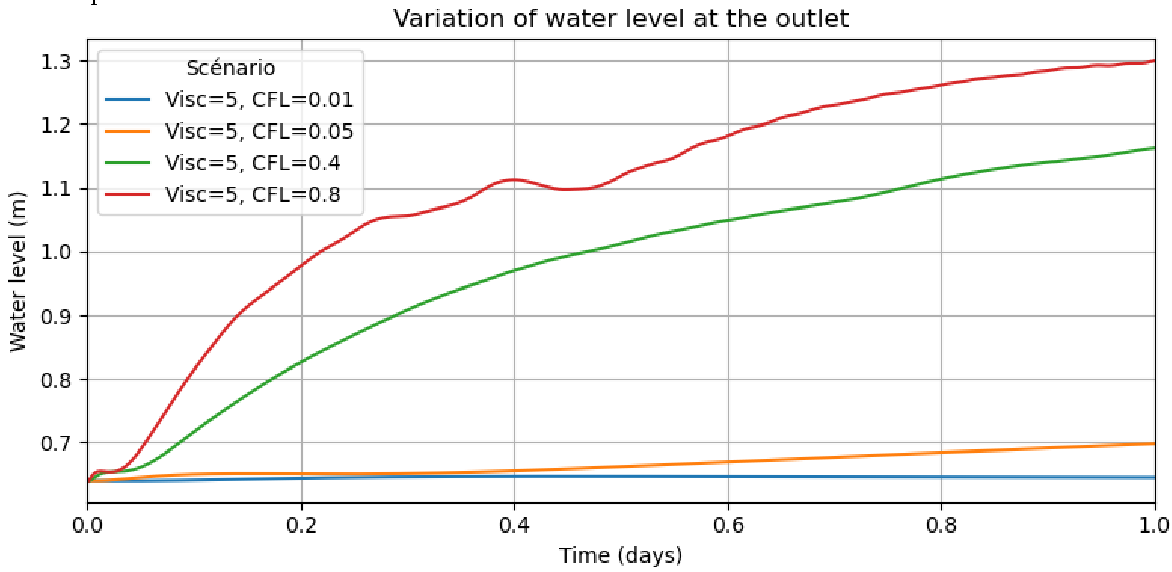

Figure 9. Variation of water depth at the outfall

The curves for CFL = 0.4 and 0.8 show a significant and continuous rise in water level, increasing from 0.64 m to approximately 1.16 m and 1.30 m, respectively, within a single day. This change of 0.52 m and 0.66 m is highly unlikely given the lake's initial volume and known inflows. Such a rapid rise would only be plausible for a much smaller body of water or an extremely high inflow rate. Therefore, despite the apparent regularity seen in the time step histograms, simulations with these scenarios exhibit masked instabilities. The perceived stability doesn't reflect the model's physical accuracy, but rather the consistency of the error.
Conversely, the curves for CFL = 0.01 and CFL = 0.05 show a minimal variation in water depth at the outfall, rising from 0.64 m to only slightly above 0.64 m and to 0.7 m, respectively. This behavior is consistent with physical expectations. Given the immense volume of the lake and the relatively small amount of water added in one day compared to that volume, we don't expect a significant rise in water level. This indicates that simulations with CFL = 0.01 and CFL = 0.05 are the most accurate and physically representative. They successfully maintain stability and reflect the very slow dynamics of the water level rise.

5.4 Analysis of mass conservation

The following curve compares the "actual change" in lake volume with the "theoretical balance" expected. The theoretical balance is calculated by subtracting the volume lost through outflows from the volume added, with this calculation performed every 10-time steps. Ideally, the "actual change" in volume should very closely match the "theoretical balance." Any deviation indicates a non-conservation of mass due to numerical errors.

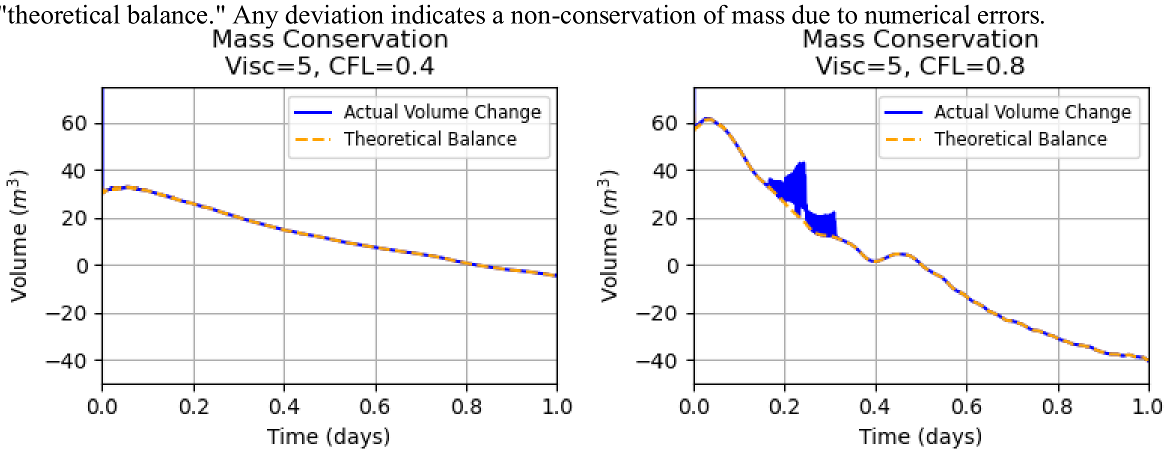

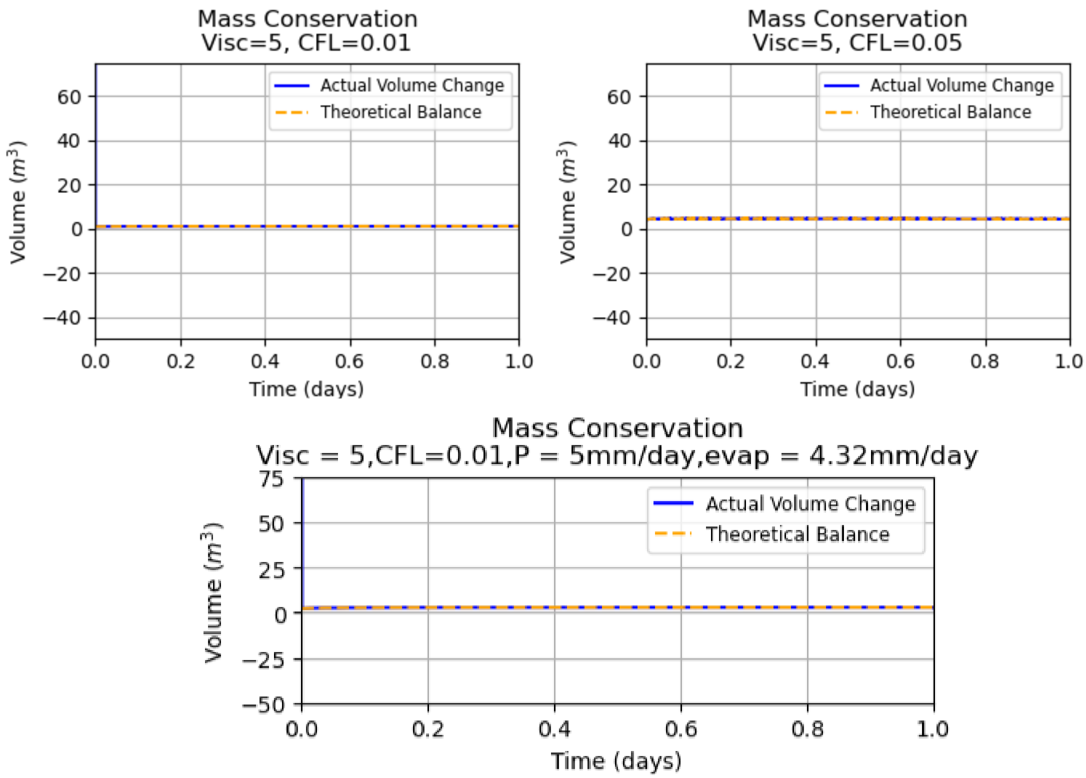

Figure 10. Actual vs. Theoretical balance of lake volume change

The analysis of the different simulation scenarios highlights the major influence of the CFL factor on mass conservation within the model. For low CFL values, specifically 0.01, 0.05, and 0.4, mass conservation is remarkably well maintained: the curves for the actual volume change closely follow the theoretical balance. This means the model neither inexplicably creates nor loses volume beyond what's accounted for by hydrological forcings and outfall discharges. It accurately tracks the defined inflows and outflows.

However, the simulation with CFL = 0.8 is not numerically stable, particularly between 1.8 and 0.35 days. The oscillations observed in the actual volume change are a clear sign of numerical instability. The model struggles to stabilize its calculations and overshoots the correct solution, erratically creating or losing volume during these short periods.

5.5 Numerical model response to tributary inflow variations

The following figure illustrates the total lake volume variation over a 1-day period for two different tributary inflow scenarios: 0.2 m³/s and 0.1 m³/s, both using a constant CFL safety factor of 0.01.

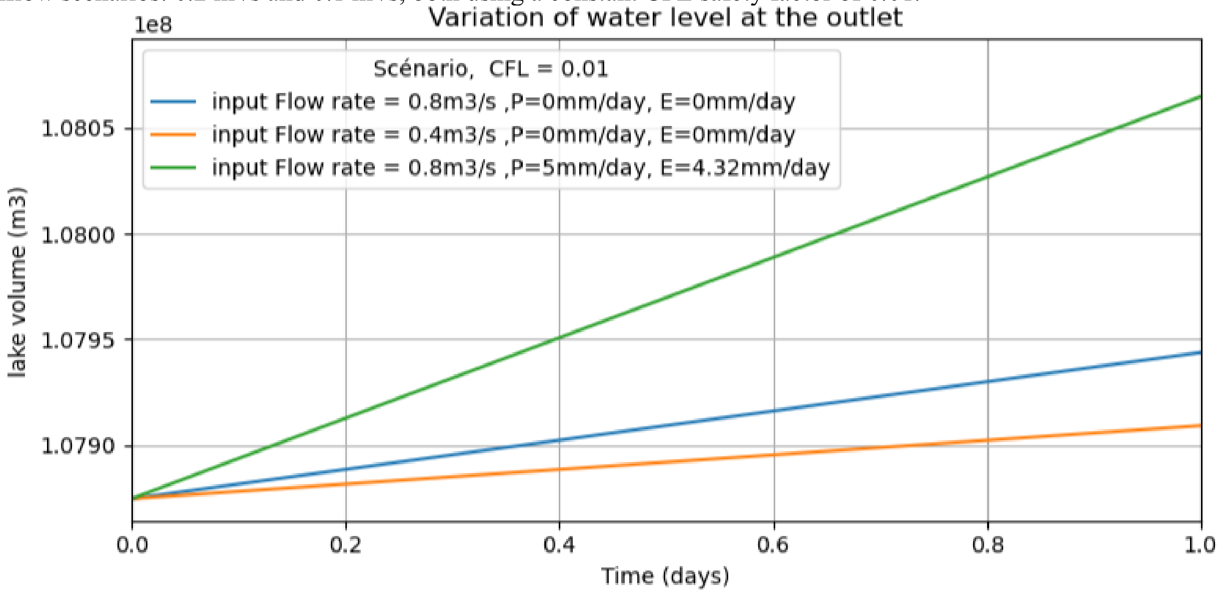

Figure 11. Evolution of Lake Volume, CFL = 0.01, with Varying Tributary Inflows, and with or without Precipitation and Evapotranspiration

This graph convincingly illustrates the numerical model's response to variations in tributary inflow over a three-day period. By representing three scenarios with a constant CFL factor (0.01) but different inflow rates (0.8 m³/s, 0.4 m³/s, and 0.8 m³/s with precipitation and evapotranspiration), the figure shows a linear increase in lake volume, perfectly consistent with the laws of mass conservation.
Furthermore, the slope of the curve is exactly proportional to the incoming flow rate: the lake fills twice as fast in the scenario where the inflow is doubled. This confirms the physical accuracy of the simulated behavior. This result not only validates the model's consistency but also the numerical stability of the simulation at CFL=0.01, which was previously identified as optimal for mass conservation.

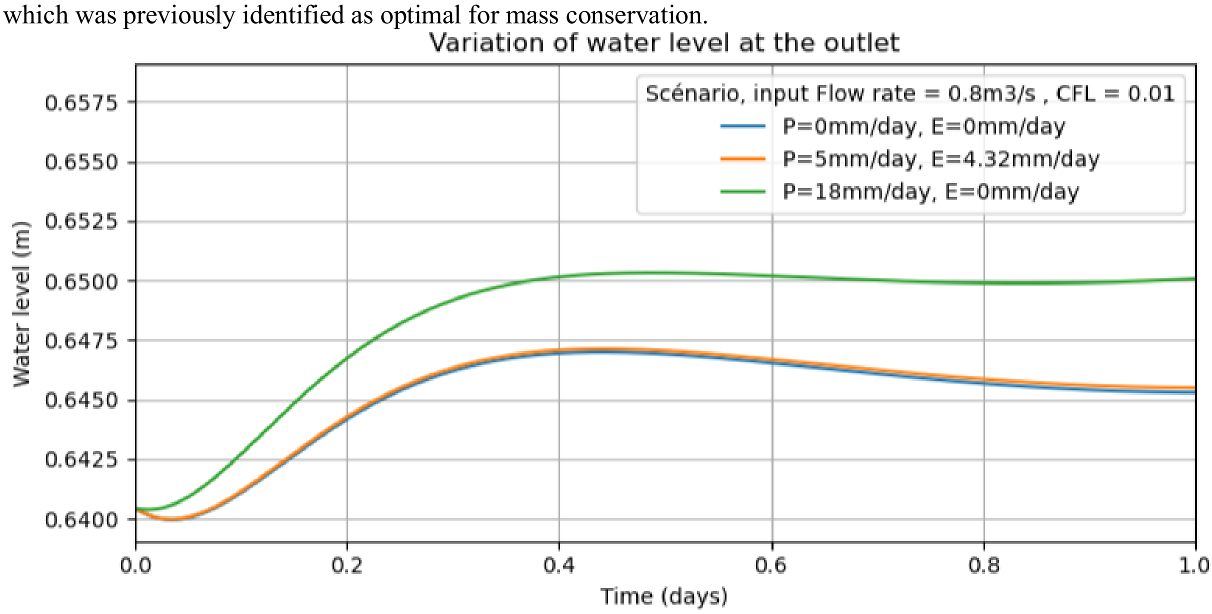

Figure 12. Variation of water level at the outfall

The figure below shows the evolution of water depth at the lake's outfall over a 1-day period. The curves differ based on the inflow rates from the tributaries.
The graph illustrating the water level evolution at the outfall reveals a very small overall variation over the three-day simulation. For scenarios without Precipitation (P) and Evapotranspiration (E), and then with P = 5mm/day and E = 4.32mm/day, the water level rise remains limited to a few centimeters, increasing from approximately 0.640 m to 0.645 m. This small variation is perfectly consistent with the lake's very large initial volume (around 108 million m³) and the moderate tributary inflows. A transient phase is observed at the beginning of the simulation, between 0 and 0.5 days, during which the water level increases more rapidly before settling into a more stable slope. The slight fluctuations reflect the model's internal hydrodynamic adjustments.

The model, with a CFL of 0.01, is clearly sensitive to variations in precipitation rates. An increase in precipitation translates to a corresponding increase in the lake's water level. This demonstrates that the hydrometeorological forcings are correctly implemented and that the model maintains its robustness and accuracy even with these additions.

5.6 Velocity at the outfall

The following figure presents a line graph illustrating the evolution of water velocity at a lake's outfall over one day, under three distinct scenarios. In all scenarios, the lake receives a constant inflow of 0.8 m³/s.

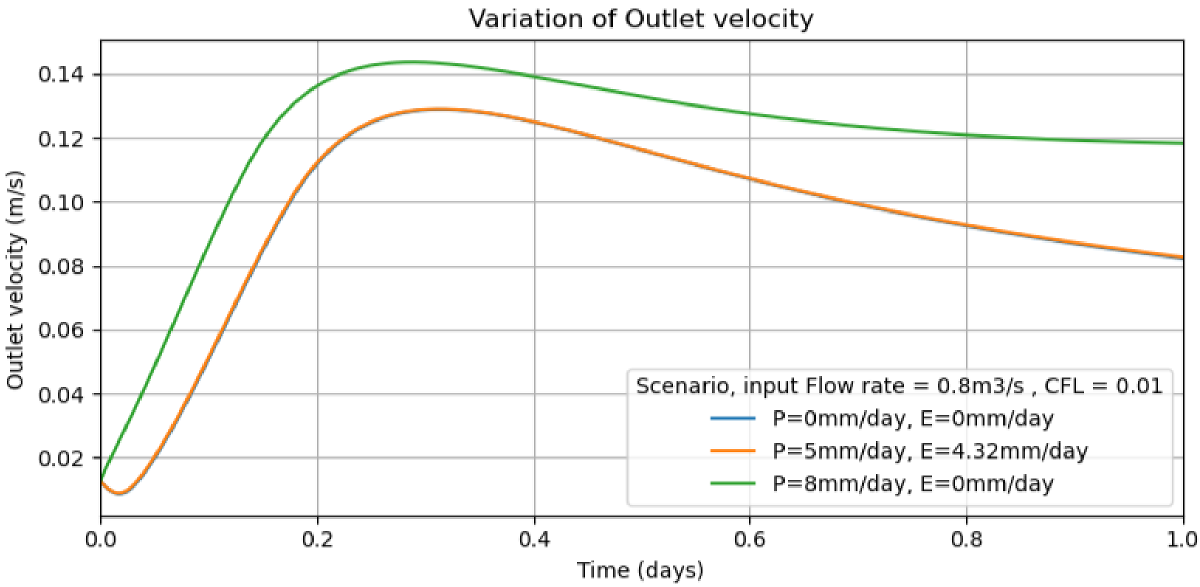

Figure 13. Variation of outlet velocity

- **Scenario 1: Input = 0.8 m³/s, P = 0, E = 0** : the outlet velocity starts at about 0.01 m/s, peaks at 0.128 m/s around 0.3 days, then gradually decreases to roughly 0.083 m/s by the end of the day.
- **Scenario 2: Input = 0.8 m³/s, P = 5 mm/day, E = 4.32 mm/day** : the curve's behavior is almost identical to Scenario 1, which suggests that the combined effect of precipitation (P) and evapotranspiration (E) has a negligible impact on the outflow dynamics.
- **Scenario 3: Input = 0.8 m³/s, P = 8.71 mm/day, E = 0 mm/day**: the velocity increases earlier and reaches a higher peak (0.142 m/s around 0.25 days), then slowly declines to finish at about 0.118 m/s.

The outlet velocity responds with a slight delay, peaking before it starts to decrease. This reflects the inertia of the lake system. When P ≈ E (Scenario 2), the net effect is almost zero, and the behavior remains unchanged. When P > E (Scenario 3), the additional water input results in a higher outlet velocity. The decrease after the peak suggests that the lake is moving towards a stable state, influenced by the initially low water level (barely reaching the 0.64m threshold).

5.7 Spatial distribution of velocity fields

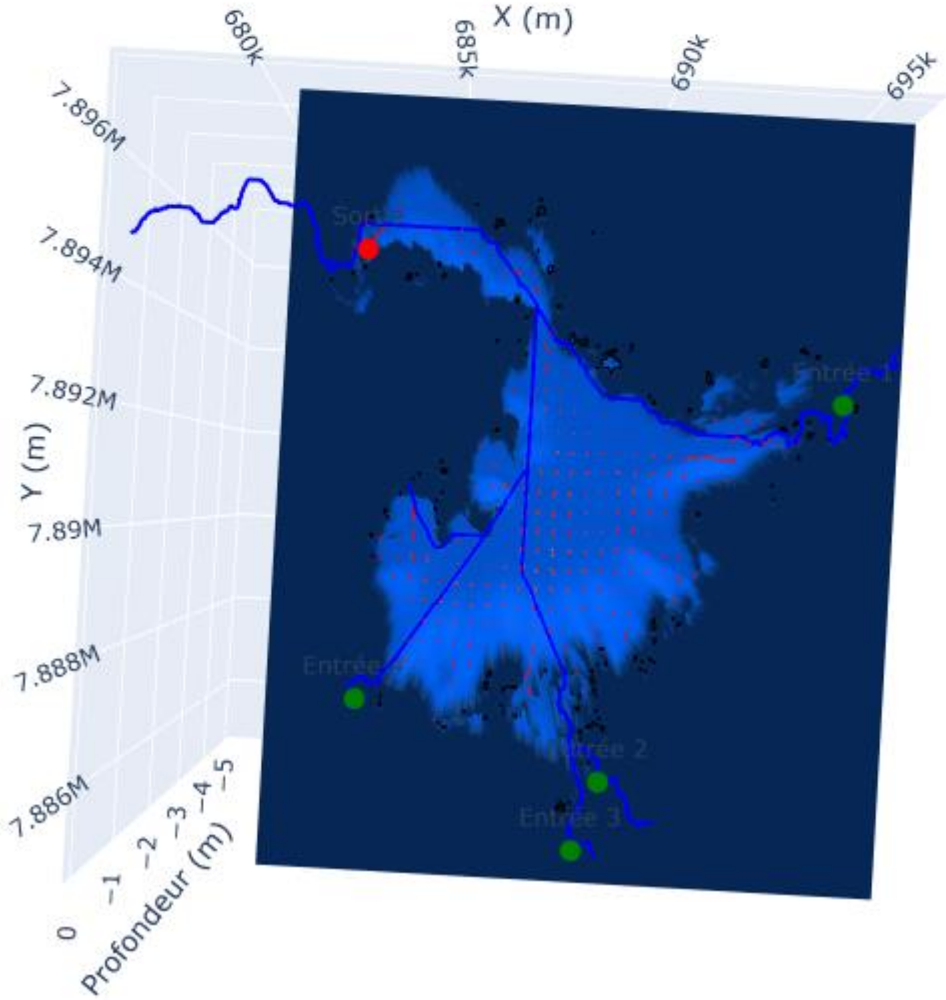

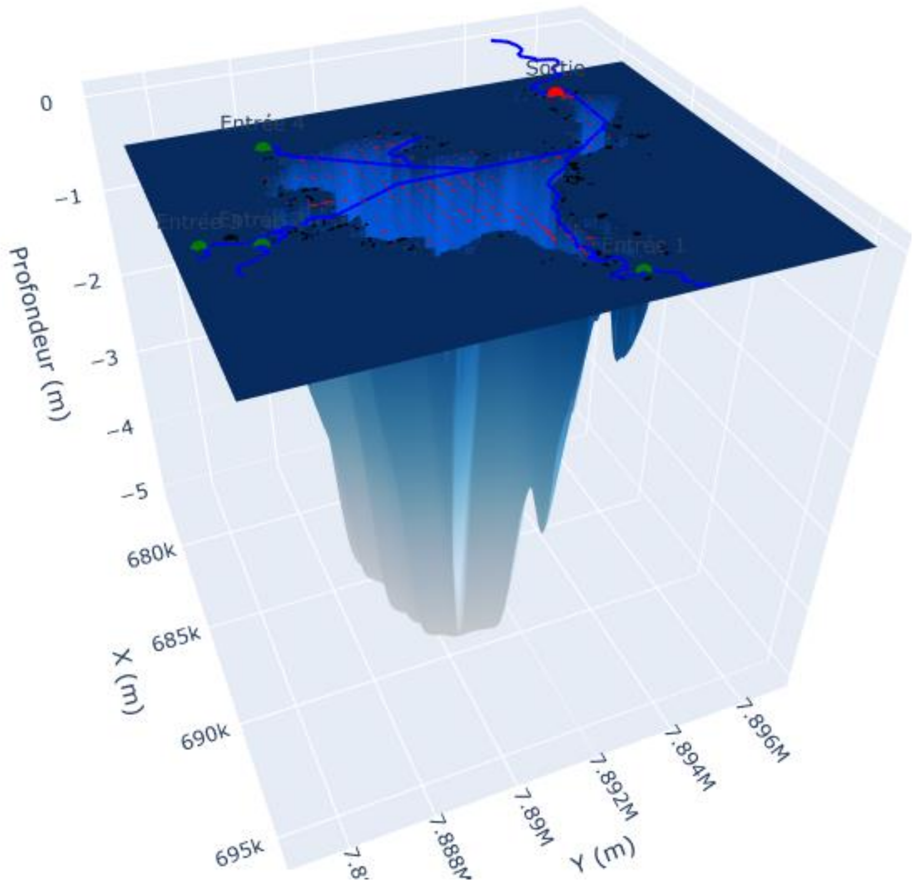

Figure 14. Surface velocity field., CFL = 0.01, Input flow = 0.2m^3/s, P = 5mm/day,E=4,32mm/day

The velocity field is visualized using red arrows spread across the lake's surface. Each arrow indicates the current's direction at a given point, with its length proportional to the water's speed. This spatial distribution of arrows reflects local variations in velocity, highlighting areas of active circulation or minimal movement. This representation allows for the observation of the simulated surface dynamics of Lake Itasy at a specific moment. It shows how water circulates from the inflow points to the outfall, while also revealing any potential areas of stagnation or mixing.

6 CONCLUSION

This work presents a rigorous study of hydrodynamic modeling for inland water bodies, focusing on Lake Itasy in Madagascar. The primary objective was to strengthen numerical stability and mass conservation, two essential elements for ensuring reliable simulations. The adopted methodology combines remote sensing (NDWI on Sentinel-2 images), geospatial analyses (SRTM DEM), and modeling based on Shallow Water Equations (SWE). The practical application to Lake Itasy adds significant value to the study. Satellite data highlighted a reduction in the lake's surface area in 2024 compared to 2023, providing relevant context for the hydrological analysis.

Comparative analysis revealed that a CFL value of 0.01 is the most effective in terms of result stability and precision. However, this configuration leads to a very high computation time, underscoring the inevitable trade-off between numerical accuracy and computational efficiency.

Furthermore, the model also accounts for major physical processes: inflow rates, precipitation, evaporation, wind effects, and management of boundary conditions at the outfall.

In summary, this work lays the foundation for a stable, precise, and physically consistent hydrodynamic model. It constitutes a valuable tool for water resource management, hydrological forecasting, and environmental studies in the Itasy region and beyond.

7 RECOMMENDATIONS AND FUTURE RESEARCH

By integrating real geospatial data and producing clear visualizations, the model we've developed stands as a relevant tool for scientific analysis and communication. In this study, we enhanced the model by incorporating the direct effects of precipitation and evaporation. Future perspectives include integrating more sophisticated formulas for calculating evapotranspiration. This will allow us to dynamically account for the influence of meteorological variables such as water surface temperature, air humidity, and wind, making the model capable of simulating complex climatic scenarios with increased precision.

Within the Institute and Observatory of Water at the University of Itasy, we are also developing an autonomous device capable of automatically measuring lake depths using a Ping2 Sonar Altimeter and Echosounder. The goal is to refine the bathymetry of Lake Itasy.

Our next study will also focus on adding a sediment transport module, including suspended load and bedload transport, and the morphological evolution of the bed via Exner's equation. This would allow us to address key issues such as lake silting and the impact of sediments on bathymetry. This extension would significantly strengthen the model's scope and accuracy, opening it up to a comprehensive study of hydro-morphodynamic processes.

REFERENCES

[1] Cea, L., & Vazquez-Cendon, M. E. (2014). A new 2D finite volume method for the Shallow Water Equations with improved robustness and mass conservation. Journal of Computational Physics, 277, 360-384.

[2] Kowalik, Z., & Murty, T. S. (2014). *Numerical Modeling of Ocean Dynamics*. World Scientific Publishing

[3] Lai, W., Chen, J., Li, Y., & Wei, R. (2017). A High-Resolution Hydrodynamic Model for Lake Circulation Driven by Wind and Inflow/Outflow. *Water*, 9(12), 929.

[4] Xia, X., Liang, Q., & Hou, J. (2017). A New 2D Hydrodynamic Model for Flood Inundation Simulations with Adaptive Mesh Refinement. *Water Resources Research*, 53(12), 10839-10854

[5] Hunter, N. M., Bates, P. D., Neelz, C. J., Pender, G., Mason, D. C., & Schumann, G. J. P. (2014). A GIS-based tool for the automatic generation of 2D hydrodynamic model meshes and input files from widely available data. *Environmental Modelling & Software*, 60, 239-250.

[6] Sheng, J., Zhu, J., Du, X., & Li, R. (2018). Recent Advances in Coastal Hydrodynamic Modeling: A Review. *Ocean Engineering*, 164, 434-455.

[7] Wang, W., Li, J., & Guo, Q. (2020). High-resolution mapping of surface water bodies using Sentinel-2 imagery and deep learning. *Remote Sensing of Environment*, 245, 111862.

[8] Pekel, J. F., Cottam, A., Gorelick, N., & Belward, A. S. (2016). High-resolution mapping of global surface water and its long-term changes. *Nature*, 540(7633), 418-422.

[9] Gholami, V., Akbari, M., Malekian, A., & Darbandi, S. (2019). Developing a robust 2D hydrodynamic model for simulating the complex flow in open channels. *Computers & Fluids*, 187, 1-13.

[10] Woodgate, D., et al. (2015). Evaluating the impact of wind stress on hydrodynamic models: A case study of Lake Windermere, UK. *Journal of Great Lakes Research*, 41(3), 738-750.

[11] Gao, S., Zhang, S., Liu, C., & Zhai, Y. (2023). Review of Recent Progress in Lake Hydrodynamic Modeling. *Journal of Hydrodynamics*, 35(1), 1-18.